Kohn and Northrup Supplemental data: Analytical methods, Ti standardization, and paleopiezometry regression.

Polished oriented thin sections were prepared perpendicular to the foliation and parallel to lineation, characteristic textures were identified, and tentative suitable areas were photographed. Samples were carbon coated and previously identified areas imaged using a Gatan MiniCL mounted on an Amray 1830 SEM, housed at the University of Idaho's Center for Electron Microscopy and Microanalysis. These images revealed unsuspected chemical and textural complexities. Many mylonites appear to contain quartz that, despite optical evidence for ductile behavior, retains relict, high-CL intensity cores (Fig. S1). We tried to avoid regions with intermixed relict cores and recrystallized rims, and instead focused on the most intensely recrystallized regions. Such regions were then microsampled by using a microscope-mounted Medenbach microdrill, producing ~3 mm diameter rounds. These rounds were epoxied into ¼" O.D. stainless steel sleeves, recoated with a relatively thick C coat, and analyzed using a Cameca IMS 3f, housed at Lawrence Livermore National Laboratory. Note that we used a C coat in part because of concern that Au coats might contain Ti. However, we did find that Ti surface contamination was present at a level of 1ppm, necessitating a modified protocol for analysis of low-Ti quartz (see following discussion).

For ion microprobe analyses, spot sizes were approximately 15x25 μm, and we analyzed masses 25.5 (rest mass), ^{27}Al, ^{30}Si, ^{40}Ca, 45.4528 ($^{91}Zr^{2+}$), ^{48}Ti, and ^{49}Ti. A mass resolving power of ~1750 was used, which discriminates the only major interference on ^{48}Ti: $^{30}Si^{18}O$. We checked for other interference problems by measuring doubly-charged Zr and $^{49}Ti/^{30}Si$, but never found any Zr interferences, and always found a $^{49}Ti/^{30}Si$ ratio that was consistent with the measured $^{48}Ti/^{30}Si$ ratio and the relative abundances of ^{48}Ti and ^{49}Ti. The other masses (^{27}Al and ^{40}Ca) were

used to monitor for contamination and microinclusions. In some samples other than those described here, we did occasionally find spikes in Al and Ca spanning mass cycles (several minutes), suggesting that we sputtered through microinclusions. Individual mass cycles that are contaminated with excess ^{40}Ca and/or ^{27}Al can be removed during data post-processing.

For low-Ti samples, Ti contamination during sample preparation can be a serious problem. We believe that coating the sample with C using a high-temperature evaporator likely contaminated surfaces slightly with Ti, possibly from metal components in the evaporator. We analyzed Herkimer "diamond" as a natural blank to monitor for such surface contamination and to determine analytical background levels. Herkimer quartz formed at 150-200 °C (Smith, 2006), so should contain c. 3±2.5 ppb Ti. Upon spot analysis of this quartz, we observed initial Ti/Si ratios corresponding to Ti levels of ~1 ppm that steadily drifted downward throughout an analysis, suggesting surface contamination. For such low-Ti quartz samples, therefore, we rastered an area roughly 150x250 μm for 15 minutes to clear away surface contamination, then reanalyzed the center of the rastered area with a focused (c. 15x25μm) spot. These spot analyses showed no drift in ^{48}Ti/^{30}Si ratios. For Herkimer quartz, we obtained an apparent concentration of 6.5-7 ppb suggesting maximum blank concentrations on the order of a few ppb. We did not make blank corrections because they would decrease the lowest two temperatures we measured for mylonites by only 4 and 1 °C respectively, and ≤0.1 °C for all other temperatures.

Converting raw ^{48}Ti/^{30}Si values requires standardization using quartz with known Ti content. Drs. Jay Thomas and E. Bruce Watson, at Rensselaer Polytechnic Institute, kindly provided experimental quartz grains that had been equilibrated with rutile (samples QTIP7 and QTIP10), and had Ti concentrations ranging from 18±6 to 200±8 ppm (2σ). We also used a natural grain of quartz from a Himalayan migmatite (LT01-15) that had a Ti concentration of

33±9 ppm. These Ti contents were determined by electron microprobe, and any systematic errors will more strongly affect LT01-15 and QTIP7 than QTIP 10. Regressing measured Ti content (in ppm) vs. raw $^{48}Ti/^{30}Si$ (each measured in cps) yielded slopes ranging from ~10150 for constrained regressions to ~10550 for unconstrained regressions (Fig. S2). The steeper slope does not intersect the Herkimer data, and is strongly influenced by the low-Ti standards LT01-15 and QTIP7. Recognizing the possibility of a small systematic error in electron microprobe analyses, we prefer a calibration of 10300±250, which essentially corresponds to a calibration that uses the QTIP10 data alone, and that is constrained to pass through the origin (Herkimer data). This implies that LT01-15 and QTIP7 have Ti contents systematically 4-5 ppm higher than measured, i.e. ~39 ppm and ~22 ppm respectively.

Propagating errors in either flow stress or, ultimately, strain rate requires accounting for uncertainties in the relationship between flow stress vs. grain size (the paleopiezometry equation), and the correlation coefficient between regressed parameters. For the paleopiezometry equation, although Stipp and Tullis (2003) regressed relevant experimental data and reported regression errors, they did not provide the correlation coefficient, so errors cannot be propagated. Note also that they regressed grain size vs. flow stress, and appear to have used a simple weighted linear regression, which accounts for errors only in Y (grain size), not X (flow stress). Their choice of grain size as a dependent variable makes sense from an experimental view in that they measured the grain size response to experimentally imposed differential stress. But natural applications involve the inverse of Stipp and Tullis' regression, i.e., estimating differential stress as a function of grain size. Consequently, we regressed $\log_{10}$(flow stress) vs. $\log_{10}$(grain size) for all regime 2 and regime 3 experimental data of Stipp and Tullis (2003) and Stipp et al. (2006), including one datum at low flow stress (W-1126/W-1116), but excluding all regime 1 data. We

70 accounted for errors in both X and Y by using the York (1966) method, as implemented in
71 Isoplot (Ludwig, 2001) v. 3.40. The resulting equation (errors at 95% confidence) is:
72 $\log_{10}$(flow stress, MPa) = (2.85±0.09) – (0.84±0.10)$\log_{10}$(grain size, μm)
73 with r^2 = 0.9132. The reciprocal of this equation is only about 1σ removed from the regression
74 equation of Stipp and Tullis (2003), but we believe our regression more accurately represents the
75 statistics of the full dataset, and allows direct application to measurements on natural samples,
76 including formal propagation of experimental errors. For grain sizes of 3-50μm, error
77 propagation results in errors in $\log_{10}$(flow stress) of ~10-20%, or ±10-50 MPa in estimates of
78 flow stress. Note that this propagated error is of the same order of magnitude as the error arising
79 from optical determination of mean grain size of recrystallized quartz (e.g. see Stipp et al., 2006).
80

Supplemental Table 1. Titanium concentrations (ppm), and $^{48}Ti/^{30}Si$ and $^{49}Ti/^{30}Si$ ratios of standards.

LT01-15

$^{48}Ti/^{30}Si$	±1σ	$^{48}Ti/^{30}Si$	±1σ	Ti (ppm)	Corr. Fact.
0.004224	0.000055	0.0003128	0.0000050	34	8049
0.003651	0.000071	0.0002374	0.0000057	34	9313
0.003880	0.000034	0.0002098	0.0000033	34	8762
0.004167	0.000031	0.0003018	0.0000029	34	8159
0.003772	0.000017	0.0002752	0.0000027	34	9014
0.004096	0.000020	0.0002971	0.0000021	34	8301
0.003413	0.000019	0.0002436	0.0000038	34	9962

QTIP10

0.019574	0.000059	0.0014435	0.0000103	205	10473
0.015494	0.000038	0.0011352	0.0000069	161	10391
0.019822	0.000074	0.0014511	0.0000100	210	10594
0.015075	0.000048	0.0011087	0.0000095	165	10945
0.017106	0.000050	0.0012595	0.0000095	187	10932
0.019258	0.000077	0.0014065	0.0000079	198	10281

QTIP7

0.002188	0.000007	0.0001628	0.0000026	18	8229
0.002175	0.000007	0.0001542	0.0000028	18	8274
0.002177	0.000006	0.0001551	0.0000025	18	8268
0.002203	0.000006	0.0001563	0.0000029	18	8173

Herkimer

8.90E-07	5.55E-08	3.76E-08	7.69E-08	0.0030	
9.12E-07	5.36E-07			0.0030	

Note: uncertainties in electron probe compositions are ±4.5 ppm for LT01-15, ±4 ppm for QTIP10, and ±3 ppm for QTIP7. Crystallization temperatures for Herkimer imply maximum Ti contents of 0.5 to 5.5 ppb.

92 Supplemental figures:

93 Fig. S1. Photomicrograph (A) and CL images (B&C) of relict quartz grain from sample CC6-9-
94 2, more representative of a bulging-recrystallization mechanism. (B) “Spallation” (likely
95 subgrain rotation) of relict grains is indicated by relatively high CL intensity cores inside regions
96 of generally low CL intensity. (C) Regions of pervasive recrystallization lack CL luminosity. (D)
97 Photomicrograph of sample CC8-3-2; bands of recrystallized quartz occur adjacent to large,
98 relatively undeformed porphyroclasts of feldspar (two large grains are at extinction). Scale bars
99 are 100 μm.
100
101 Fig. S2. Ti content of standards vs. raw $^{48}Ti/^{30}Si$ ratios. Unconstrained regressions imply a slope
102 of ~10550. Specifying a zero intercept (consistent with Herkimer measurements) implies a slope
103 of ~10160. High-Ti data are least susceptible to systematic analytical errors, and imply a slope of
104 ~10320. A slope of 10300±250 was used for interpreting natural mylonites.
105

Fig. S1 Kohn & Northrup

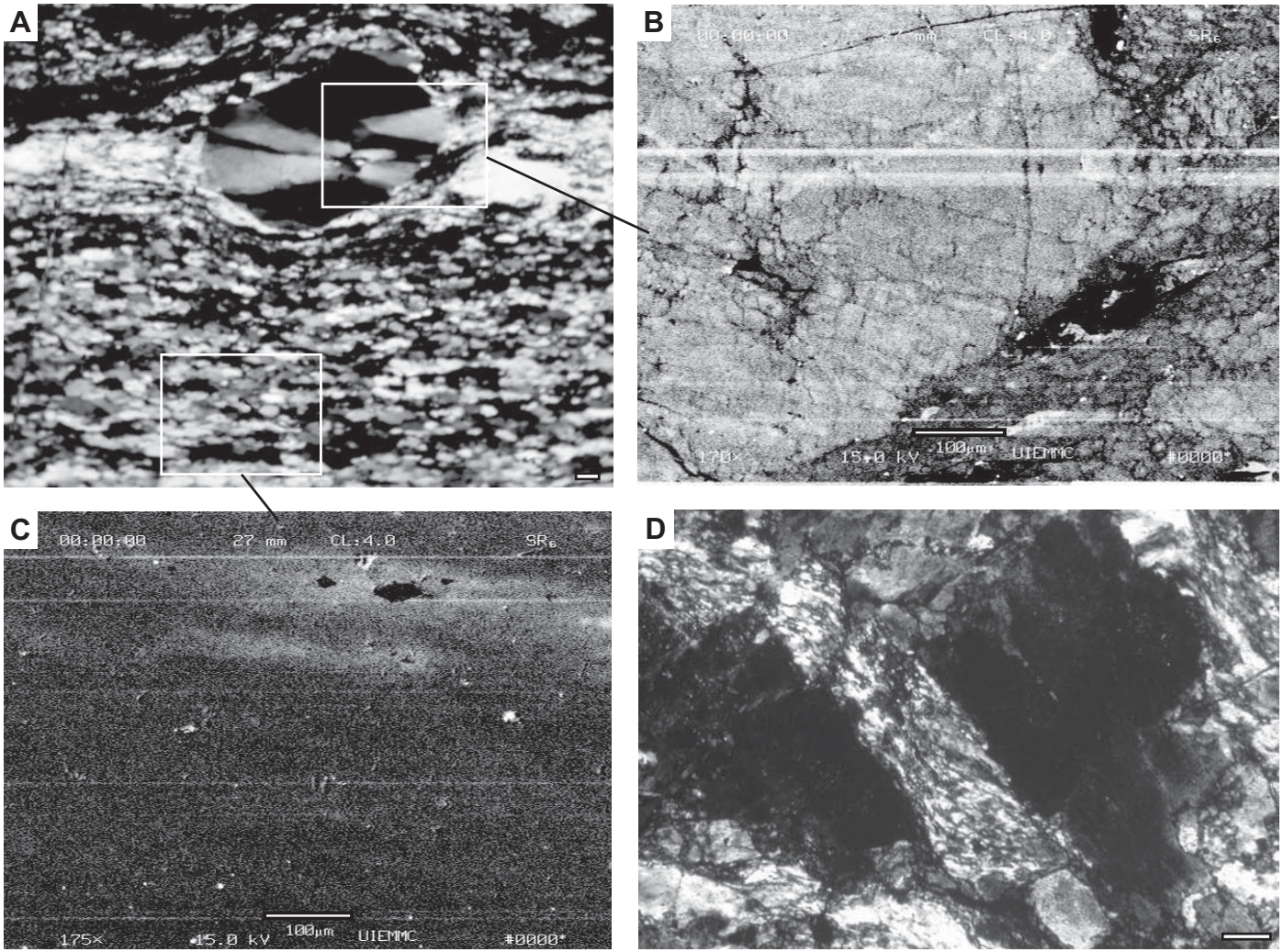

Supplemental Fig. 2
Kohn and Northrup